



0017-9310(95)00105-0

Transient three-dimensional natural convection in a rectangular enclosure

SHOU-SHING HSIEH and SHYH-SHYAN YANG

Department of Mechanical Engineering, National Sun Yat-Sen University, Kaohsiung, Taiwan 80424, Republic of China

(Received 2 November 1994 and in final form 27 February 1995)

Abstract—An experimental study is presented for transient buoyancy-induced natural convection in the Rayleigh number range of 6.9×10^7 – 4.12×10^8 for aspect ratios of $A_H = 3$ and $A_w = 1.2$ inside a rectangular enclosure with silicone oil as the working medium wherein the two vertical walls were heated on the right wall and cooled on the left wall as $t \geq 0$, respectively. The remaining four walls were adiabatic. Time evolution of streak flow patterns was observed and temporal temperature distributions are presented and analyzed. In addition, the present results are compared with previous two-dimensional experimental and three-dimensional numerical results.

1. INTRODUCTION

Bouyancy-driven fluid flow analysis in enclosures has many thermal engineering applications, such as heating and cooling of buildings, cryogenic storage tanks, the cooling of electronic components and solar energy collectors. In the design of such devices, the transient behavior of flows is of vital interest in order to assess, for example, the maximum heat transfer rates. The transient flow properties may differ significantly from the steady-state values. In the present paper, an experimental study is conducted on three-dimensional transient natural convection in a rectangular enclosure.

It is obvious that convection flows, as well as fluid motion in general, are three-dimensional. However, the limitations of mathematical analysis and experimental techniques have led to a very common trend of approximating convection flows by two-dimensional models. The experimental simulation and mathematical modeling of two-dimensional convection flows have created many flow structures that do not appear to be comparable with real, three-dimensional flows. Therefore, the data presented herein should be useful in three-dimensional numerical code validation and the assessment of the assumption of two dimensions in previous experimental studies. To the authors' best knowledge, comprehensive and thorough data for time-dependent three-dimensional natural convection in enclosures are not available in the literature. For a numerical study, Schladow *et al.* [1] reported a series of two- and three-dimensional numerical simulations of transient flow in a side-heated cavity at $Ra = 2 \times 10^9$. Fusegi *et al.* [2] numerically studied transient three-dimensional natural convection in a differentially heated cubical enclosure at a typical Rayleigh number of 10^9 . They illustrated time evolutions of the temperature and flow.

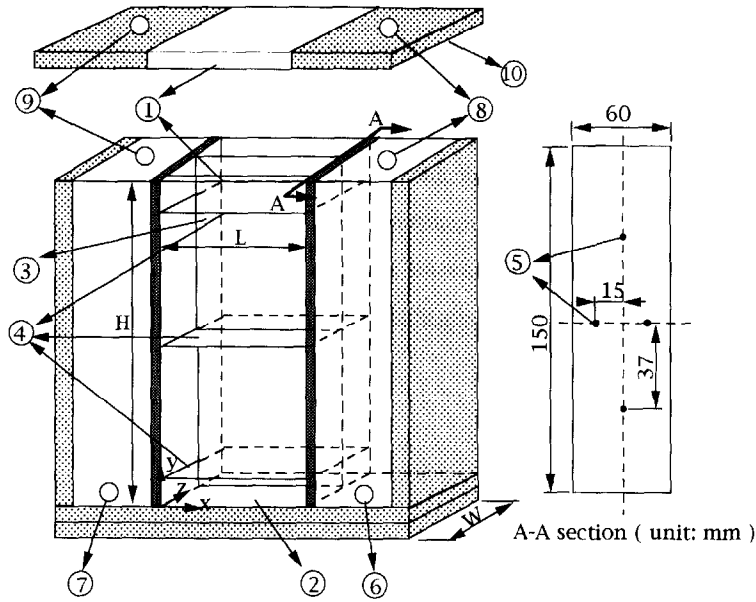
In the present work, transient three-dimensional natural convection experiments in a rectangular enclosure, shown in Fig. 1, with differentially heated vertical walls were carried out for a range of Rayleigh numbers, $6.9 \times 10^7 \leq Ra \leq 4.12 \times 10^8$, and for $Pr \cong 457$ for lateral aspect ratio $A_w = 1.2$ and $A_H = 3$. With these parameters, the flow is expected to be three-dimensional and time-dependent. The present work is a direct extension of previous three-dimensional steady-state experiments [3]. The primary objective of this study is to present complete three-dimensional pictures of the gross features of a time evolving convective pattern in the rectangular enclosure. Time-dependent changes in the thermal characteristics and heat transfer rate in the enclosures as well as flow characteristics through flow visualization are obtained.

The three-dimensional experimental results of the present study may provide useful and systematic data for this type of flow and, moreover, examination of the data permits closer analyses of transient three-dimensional features. For instance, both quantitative and qualitative information for the thermal boundary layer stabilizing time will be noted in the present experimental results.

2. EXPERIMENTAL SETUP AND PROCEDURE

2.1. Experimental facility

The thermal convection flow was generated in a $150 \times 50 \times 60$ mm rectangular enclosure. Figure 2 shows the enclosure and the coordinate system used. The y direction is vertically upwards. Two opposite lateral walls of the box ($x = 0$ and $x = L$) were made of copper (5 mm in thickness) and kept at a prescribed constant temperature by two isothermal baths. The four other walls, made from 10 mm Plexiglas with 10



- | | |
|--|-------------------------------------|
| (1) test section | (6) hot water inlet |
| (2) 10mm plexiglass | (7) cold water inlet |
| (3) the vertical(xy) plane at $z=0.5W$ | (8) hot water outlet |
| (4) the horizontal(xz) plane $y=0.9H, 0.5H$ and $0.1H$ | (9) cold water outlet |
| (5) wall temperature measurement position(at two opposite vertical walls) | (10) top ceiling of the enclosure |



-  10mm thickness polystyrene foam thermal insulator
 5mm thickness copper plate

Fig. 2. Schematic of the test section.

less than 3°C . The experiment was started by simultaneously pumping hot demineralized water at temperature T_H and cold demineralized water at temperature T_C from these two baths into the respective end water jackets. The temperatures in the jackets were subsequently maintained to within about 0.1°C of their respective values. This combination of pumping water already at the desired temperature and the rapid heat transfer through the thin copper end walls (5 mm) enabled the end walls to be brought to temperature in timescales $t_w < t_b$, as desired. With this, an initiation timescale of less than 5 s is achieved. Suitable values of T_H and T_C were chosen to minimize the temperature difference between the mean enclosure temperature and the ambient. The temperature differences between the heated and cooled walls was varied in the range $10\text{--}60^{\circ}\text{C}$ and the ambient temperatures were kept at 25°C . The enclosure was filled with silicone oil as working fluid for each experimental run. The effects of variable properties of the fluid on natural convection have been investigated previously [4, 5]. In the case of a liquid medium like silicone

oil, the temperature dependence of viscosity can be important. This can be seen from Table 1.

Five copper/constantan thermocouples were installed at various locations on each of the two (heated/cooled) vertical walls. The maximum temperature deviation from the mean temperature of the wall was $\pm 0.1^{\circ}\text{C}$ and the accuracy of all thermocouple measurements was $\pm 0.2^{\circ}\text{C}$. A very thin (AWG 40) thermocouple probe was inserted through a slot in the top ceiling of the enclosure, fixed at a different height, and chosen in the horizontal or lateral direction to measure the local temperature of the cell.

2.2. Flow visualization

Flow structures were visualized using photographic records of the motion of tracer particles illuminated by a sheet of white light. Aluminum powders were used as tracer particles. The typical size of the particles was $5\text{--}15\ \mu\text{m}$ and their concentration in the working fluid was kept below 0.1% by weight. Time-exposure (25–30 s) streak photographs of the evolving flow field were taken of the flow patterns using a Cannon-AE1

Table 1. Physical properties of the silicone oil used

Temperature [K]	Viscosity [m ² s ⁻¹]	Thermal conductivity [W m ⁻¹ K ⁻¹]	Thermal diffusivity [m ² s ⁻¹]	Specific heat [kJ kg ⁻¹ K ⁻¹]	Prandtl number
298	50 × 10 ⁻⁶	0.154	1.06 × 10 ⁻⁷	1.52	472
303	47.9 × 10 ⁻⁶	0.1538	1.05 × 10 ⁻⁷	1.532	457
308	45.8 × 10 ⁻⁶	0.153	1.03 × 10 ⁻⁷	1.544	444
313	43.7 × 10 ⁻⁶	0.1529	1.02 × 10 ⁻⁷	1.556	427
318	41.5 × 10 ⁻⁶	0.1524	1.01 × 10 ⁻⁷	1.568	410
323	39.4 × 10 ⁻⁶	0.1519	1 × 10 ⁻⁷	1.58	394
328	37.3 × 10 ⁻⁶	0.1514	0.99 × 10 ⁻⁷	1.592	377
333	35.2 × 10 ⁻⁶	0.151	0.98 × 10 ⁻⁷	1.604	345
338	33 × 10 ⁻⁶	0.1505	0.97 × 10 ⁻⁷	1.616	340

camera with Fuji black and white ISO 100 films. The streak photographs give an integrated picture of the flow field over the period of exposure.

3. DATA REDUCTION AND UNCERTAINTY

The local values of the thermophysical properties of the working fluid in the enclosure were obtained at a reference temperature referred to as a mean bulk temperature of

$$T_m = 0.5(T_H + T_C). \quad (1)$$

The length scale used in calculating the Rayleigh number was $H = 150 \text{ mm} \pm 0.5\%$. The temperature difference used in driving the Rayleigh number is the difference in temperature of hot and cold walls, i.e. the overall temperature difference. The major dimensionless parameters that determine the structure of a constant property flow in a differentially heated enclosure are the Rayleigh number,

$$Ra = \frac{g\beta(T_H - T_C)H^3}{\alpha\nu} \quad (2)$$

the Prandtl number and the enclosure aspect ratio.

Cooling and heating water flow rates (steady state), nominally 680 kg h^{-1} , are measured with a rotameter, calibrated by a stop watch-and-bucket method to within $\pm 3\%$ for temperatures near ambient. The highest temperature the walls were operated at was about 60°C . The flow meter tended to read high by about 3–5%, in addition to a decrease of approximately 2% in the fluid density. Partially offsetting those two uncertainties is an error that increases about 3% at 25°C owing to non-linearity of the temperature difference measuring period. Data are not corrected for conduction through the neoprene gasket from a heated wall to a cooled wall (about 5%), or for radiation heat transfer from the hot wall to the cold wall (about 2%). Insulation effect was examined for the worst case (i.e. $\Delta T = 60^\circ\text{C}$). It was found that the maximum heat loss was about 5%. Overall heat balance in the test section (total measured heat transfer from hot wall minus total measured heat transfer to the cold wall divided by total measured heat transfer from the hot wall) was typically between $\pm 3\%$ (for

the highest Rayleigh number) and $\pm 5\%$ (for the lowest Rayleigh number) for steady state. In spite of this, the overall heat transfer measurements were expected to be within $\pm 5\%$ of the actual convection heat transfer from each wall. Based on the aforementioned relevant uncertainties and following Hsieh and Wang [3], the maximum estimated uncertainties in Ra and Nu are 7 and 10%, respectively.

4. RESULTS AND DISCUSSION

4.1. Characteristics of the flow

Time evolutions of the temperature and flow fields at $Ra = 4.12 \times 10^8$ were examined by using three-dimensional perspective views of the flow field.

4.1.1. *Midplane* ($z = 0.5W$). Figure 3 contains a series of streak typical photographs for $Ra = 4.12 \times 10^8$, $A_w = 1.2$ and $A_H = 3$ showing the transient flow field from initiation to steady state. Observation over time allows a description of the flow evolution. The hot wall is on the right-hand side in all figures. While there is a general symmetry in each picture, the most striking features of the flow field are both its complexity and the rapidity with which it evolves. Figure 3 (a)–(h) shows the development of the flow at $y = 0.9H$, $0.1H$ (both in the xz plane) and $z = 0.5W$ and $A_w = 1.2$ for $A_H = 3$, beginning at an elapsed time of 30 s [Fig. 3(a)] and ending at 5 h [Fig. 3(h)]. The timing of the figure is more widely spaced in Figs. 3(d)–(h) to allow the development to near steady state to be obtained. Initially, the fluid is at a uniform temperature of T_0 and motionless. A sudden differential heating at $t \geq 0$ at two vertical side walls ($x = 0$ and L) created sharp temperature gradients in the proximity of the isothermal walls. In the central region of the enclosure, the fluid is still at the initial uniform temperature; thus, the heated fluid near the side wall $x = L$ starts to rise, and the cooled fluid near $x = 0$ moves downwards. Subsequent to this initial development, the heated and cooled fluids flow along the ceiling and floor of the enclosure, respectively, in the opposite directions. This sequence shows formation of a big anticlockwise eddy in the vertical mid-plane ($z = 0.5W$). One minute later [Fig. 3(b)], the circulation is already moving towards the hot wall. The

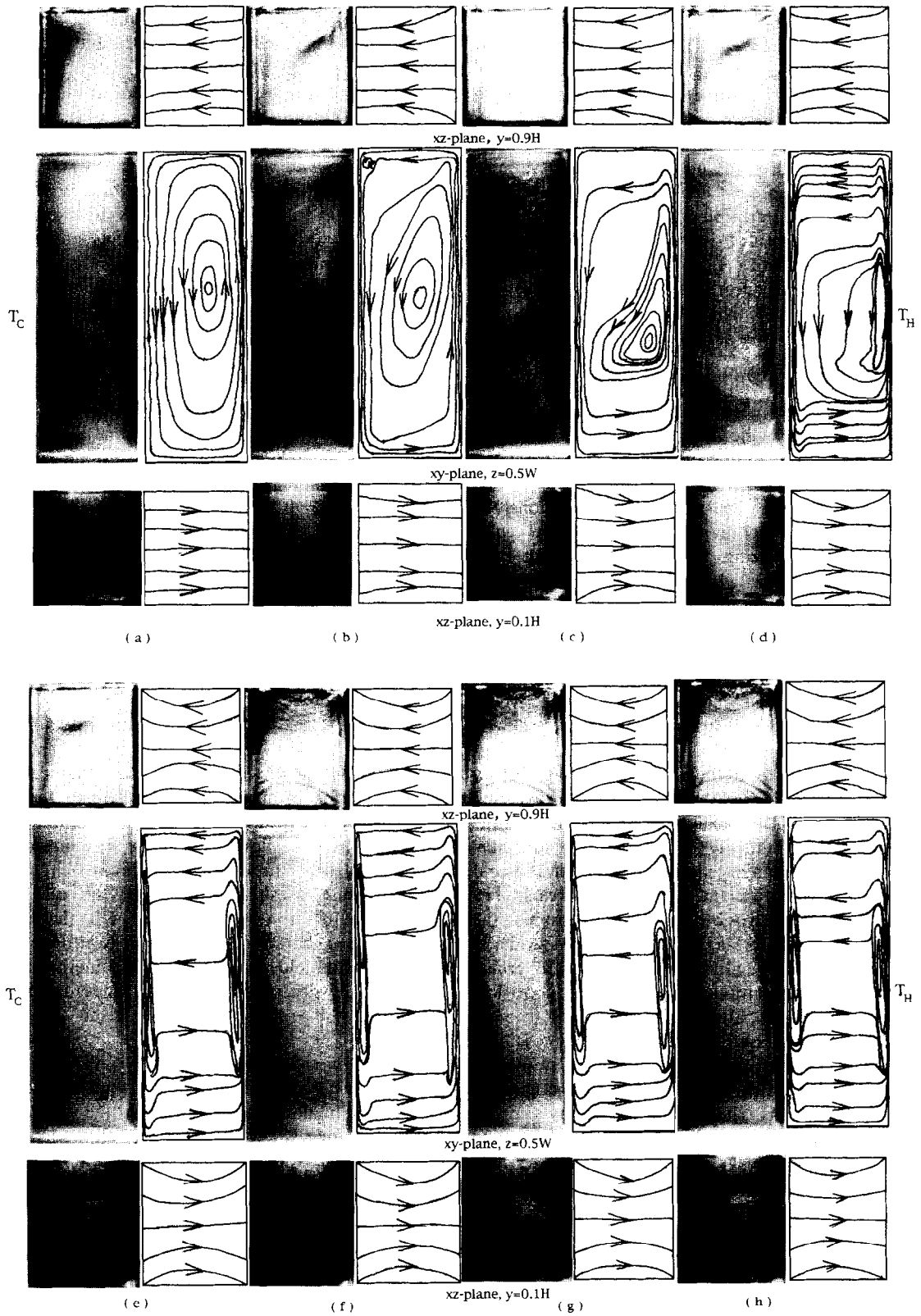


Fig. 3. Streak photographs of the transient flow with $A_w = 1.2$, $A_H = 3$ and $Ra = 4.12 \times 10^8$: (a) 30 s; (b) 90 s; (c) 240 s; (d) 10 min; (e) 0.5 h (f) 1 h; (g) 2 h; (h) 5 h.

situation persists until Fig. 3(e) in which the eddy breaks up, and in Fig. 3(f) two small eddies appear near the hot and cold walls, respectively. The flow subsequently evolves somewhat more regularly, until one observes the near steady picture in Fig. 3(f).

The asymmetry of the flow pattern (in the xy plane) shown in Fig. 3(b)–(d) may be caused by variable viscosity in the present experiments, which resulted in the cells and intrusion traveling upwards. This is because the smaller viscosity in the portion close to the hot wall leads to a larger upward velocity than the downward velocity near the cold wall. This intrusion, as well as the traveling cell, causes a transient temperature distribution as evidenced by the later temperature history which also, in turn, induces the viscosity to change with time and space. The present variable viscosity effect due to temperature change therefore results in the flow unsteadiness under study.

Figure 3(b) shows that the intrusion has split at the upper corner of the cold wall into two distinct streams: one, the hottest fluid, traveling along the ceiling, and the other diverging forwards to the center of the cavity, forcing the anticlockwise cell back towards the hot wall. In addition, a clockwise eddy in the split region is also evident. This phenomenon becomes more obvious [Fig. 3(c)] as time increases. At 10 min [Fig. 3(d)], the split in the intrusion has penetrated back to the divergence and the anticlockwise cell has become small and intensified. It has begun migrating to the hot wall. The weak clockwise circulation shown in Fig. 3(b) has virtually disappeared. The interior of the enclosure is being filled by separated intrusion and the sharpness of the diverging flow is retained. The remainder of the flow follows the pattern. By 30 min [Fig. 3(e)], a distinct ‘lobe-like’ recirculation area adjacent to both the hot and cold wall regions maintains the two intrusion streams. The layering by the intrusion ultimately almost fills the entire space. The streak photograph shows evidence of vertical flow reversal as the upper half of the vertical boundary layer detains; the lower-half core flow remains essentially parallel as it is entrained.

As time progresses, the layered intrusion is substantially accomplished, with a resulting near-stagnant interior core, except for the two regions near the hot and cold walls. The reason for this may again be the variable viscosity of the present liquid working medium which breaks the symmetry of the flow pattern. As mentioned earlier, due to an unsteady temperature distribution the viscosity may change with time and space. The unsteadiness near the hot/cold walls shown in Fig. 3 (f) and (g) seems to be a result of interaction between buoyancy and shear force [6] but this effect decreases as time increases. Finally, the photograph of Fig. 3(h) clearly demonstrates the combined structure of the distinct boundary layers and the near-stagnant interior core when the flow approaches steady state. The time evolutions of the flow fields portrayed above are qualitatively consistent with those reported by Kublbeck *et al.* [7],

who considered a two-dimensional square enclosure. Three-dimensionalities are only near the end walls. It is worth noting that areas of weak vortices are found in the regions near the isothermal vertical side walls ($x = 0$ and L) and the adiabatic vertical end walls ($z = 0$ and W).

4.1.2. *Horizontal planes* ($y = 0.9H$ and $y = 0.1H$). Figure 3(a)–(h) also shows the time evolution of the flow pattern at $y = 0.9H$ and $0.1H$. Away from the centerplane ($y = 0.5H$), the flow is strongly influenced by a three-dimensional effect. The flow is clearly different from that at the centerplane (not shown), with flows actually occurring within a region close to the vertical end walls ($z = 0$ and W). It also shows the end wall exerting a very large effect on the flow field. This is because of the traverse flows (in the z direction), which are noticeable in Fig. 3(a)–(h) in the enclosure, and a direct manifestation of the three-dimensional nature of flow. Also, the flow appears to be spiraling from the rear and front walls to the plane of symmetry ($z = 0.5W$). There the flow follows outwardly directed helical paths, then in the outer wall regions it spirals to the front and rear walls, respectively, and finally the motion is transformed into an inward spiral directed to the focal points on these walls. This can be seen from the concave streak photographs of Fig. 3(a)–(h). This lateral motion may also be due to the effect of variable properties of the present working medium.

In summary, the dynamic development and stability of the convection were studied in the range $6.9 \times 10^7 \leq Ra \leq 4.12 \times 10^8$. It was found that a sudden application of a temperature difference to the side walls of a cubical rectangular enclosure induces a strong convection flow immediately. The flow and temperature fields (discussed later) approach their final structure within 30 min. For the case of $Ra = 4.12 \times 10^8$ at $A_H = 3$ and $A_w = 1.2$, the final steady state is characterized by two cells in the mid-plane near hot/cold walls, while in the intermediate states a single vortex occupying almost the entire core is observed.

4.2. Temperature history

4.2.1. *The early phase* ($t \leq 15$ min). Figure 4 shows time evolution along the x direction at the midplane ($z = 0.5W$) for $t \leq 15$ min at different elevations for three different Rayleigh numbers. Starting with $Ra = 6.9 \times 10^7$, Fig. 4(a) at $t = 1$ min shows that near the hot/cold walls, the temperatures are nearly stratified. At this stage, the temperatures existing in the interior core region at different elevations strongly suggest that the existence of the hot fluid is not felt and, consequently, the central zone was found to be ‘inactive’ (for instance, $y = 0.5H$). However, vivid flow motion shown in Fig. 3 provides convection near hot/cold walls as well as the top ceiling and the bottom floor (for instance, $y = 0.1H$ and $0.9H$) resulting in the magnitude of temperature having the following sequence, i.e. $\theta|_{y=0.9H} > \theta|_{y=0.1H} > \theta|_{y=0.5H}$, which is

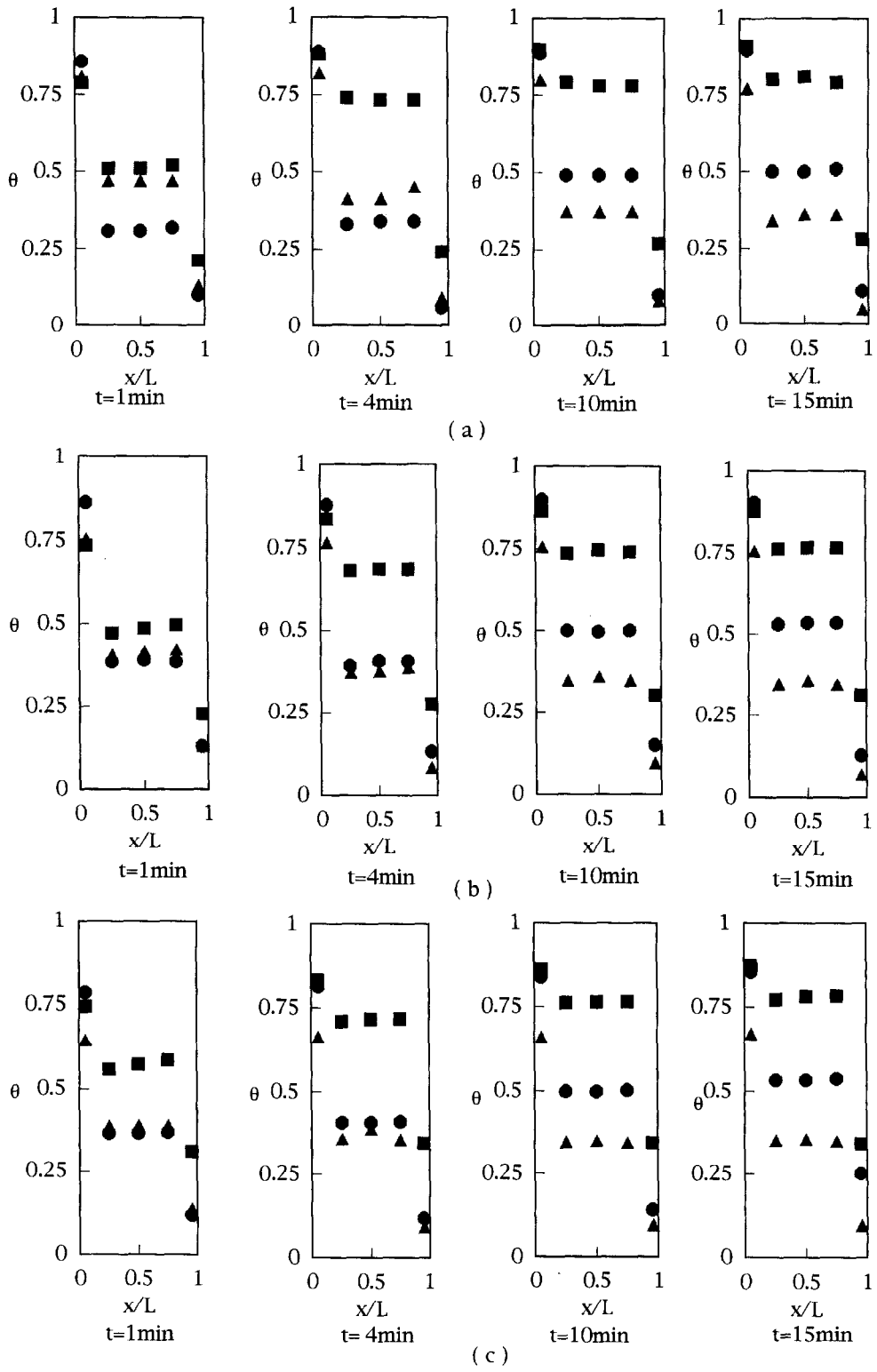


Fig. 4. Midplane ($0.5W$) temperature history ($t \leq 15$ min) for $A_w = 1.2$ and $A_H = 3$ at (■) $y = 0.9H$, (●) $y = 0.5H$ and (▲) $y = 0.1H$ for three different Rayleigh numbers: (a) $Ra = 6.9 \times 10^7$; (b) $Ra = 1.38 \times 10^8$; (c) $Ra = 4.12 \times 10^8$.

not stable. This situation persists until $t > 4$ min which can be seen from Fig. 4(a) for $t = 10$ and 15 min. As the Rayleigh number increases, this change happens earlier, which is shown in Fig. 4(c) at $t = 4$ min, and the temperatures in the core region eventually become thermally stratified ($t = 15$ min). Generally speaking, for Fig. 4(a)–(c), it strongly indicates that there are

two regions inside the enclosure. One is an ‘active region’ and the other is an ‘inactive region’, as stated earlier. The active region occupies a small part of the enclosure which is in the vicinity of the heated/cooled walls and horizontal walls.

Figure 5 shows time-dependent temperature distributions corresponding to a centered plane

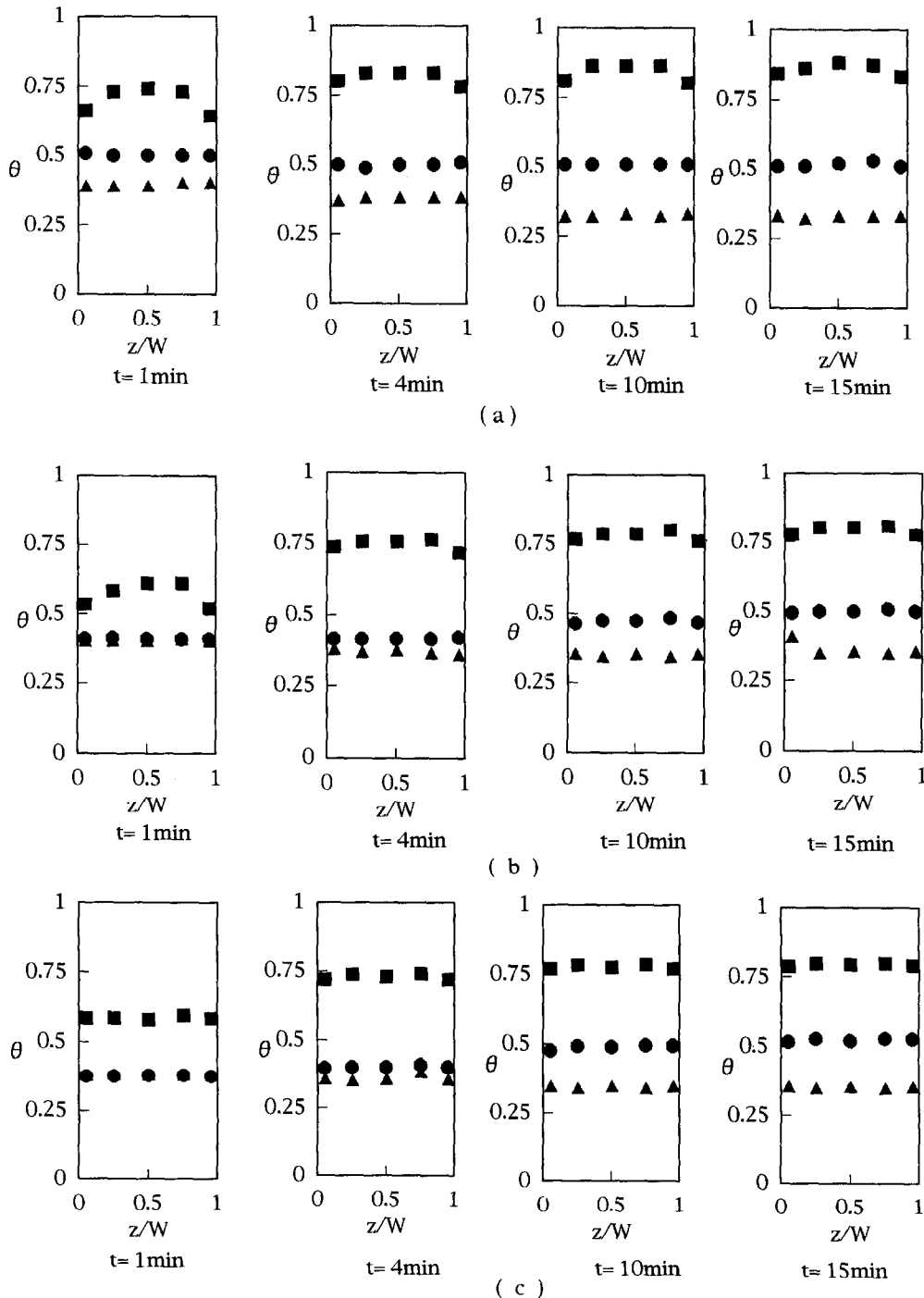
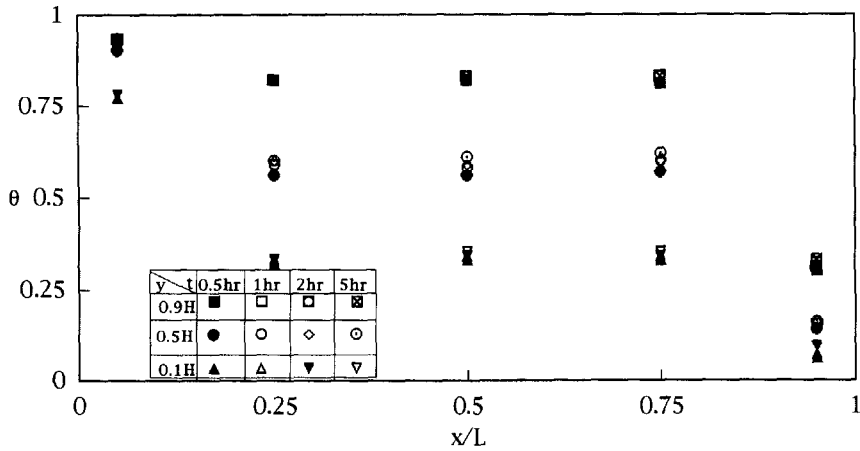


Fig. 5. Centered plane ($x = 0.5L$) time-dependent temperature distribution ($t \leq 15$ min) for $A_w = 1.2$ and $A_H = 3$ at (■) $y = 0.9H$, (●) $y = 0.5H$ and (▲) $y = 0.1H$ for the three different Rayleigh numbers: (a) $Ra = 6.9 \times 10^7$; (b) $Ra = 1.38 \times 10^8$; (c) $Ra = 4.12 \times 10^8$.

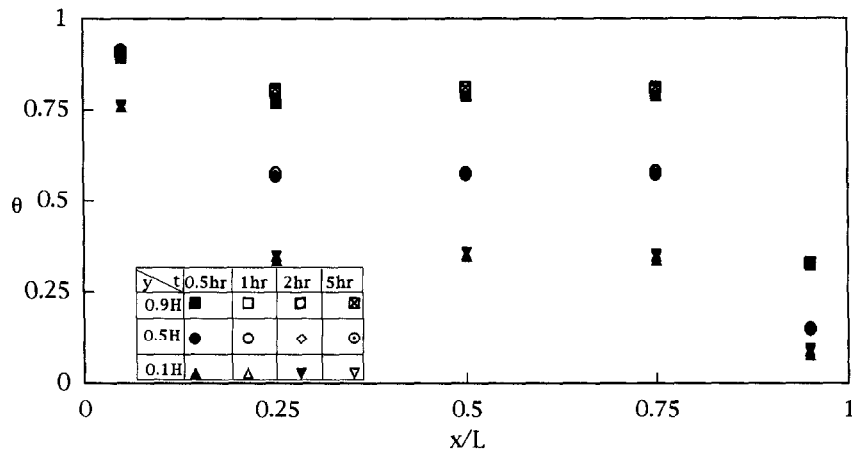
($x = 0.5L$) parallel to the hot/cold walls. Comparing Fig. 5(a)–(c), the heat transport becomes strong as the Rayleigh number increases, especially at $y = 0.9H$. Figure 5(a)–(c) are similar and provide some evidence for the result that throughout most of the enclosure the temperature field is practically two-dimensional

because it is independent of the z direction and it is linearly stratified in the vertical direction as time $t \geq 15$ min.

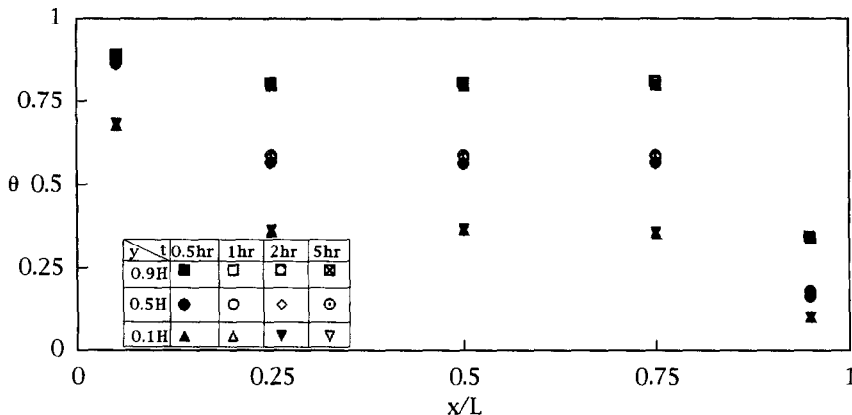
4.2.2. *The subsequent phase ($0.5 \leq t \leq 5$ h; steady state).* Figure 6 shows the vertical temperature distribution in the core of the enclosure at $0.5 \leq t \leq 5$



(a)



(b)



(c)

Fig. 6. Midplane ($z = 0.5W$) temperature history ($0.5 \leq t \leq 5$ h) for $A_w = 1.2$ and $A_H = 3$ at $y = 0.1H, 0.5H$ and $0.9H$ for three different Rayleigh numbers: (a) $Ra = 6.9 \times 10^7$; (b) $Ra = 1.38 \times 10^8$; (c) $Ra = 4.12 \times 10^8$.

h for three different Rayleigh numbers. The stable thermal stratification was obtained at $t \geq 0.5$ h. As the Rayleigh number increases convection dominates and, furthermore, temperature inversions were also observed and are shown in the central portion ($0.125 \leq x/L \leq 0.9$) of Fig. 6(c) at $y = 0.5H$. These inversions suggest that the flow immediately adjacent to the vertical walls is so strong that it produces a high rate of tangential convection along the heated wall compared with the vertical transport of heat from the surface of the heated wall across to the cooled wall. At this stage ($t \geq 0.5$ h) simultaneous conduction in the core of the enclosure is actually opposite to the overall direction of heat flow. This behavior is similar to the results of a previous study in the steady state [3]. Following Fig. 7, one may observe the steady state reached at $t \geq 0.5$ h. The thermal stratified state was dominant over the entire space. Again, Figs. 7(a)–(c) are remarkably similar and the temperature field is two-dimensional.

4.3. Duration of the thermal layer development (t_b)

The duration of the thermal layering of the present transient experiment, Fig. 8, can be predicted approximately by the scaling statement reported in refs. [8, 9] for a two-dimensional enclosure. Following the theory, the horizontal boundary layer development should be complete when

$$t^+ \sim \left(\frac{H}{L}\right)^{-1} Ra^{-1/4} \quad (3)$$

where t^+ is dimensionless time [$t/(H^2/\alpha)$], based on the vertical boundary layer (δ) which has an order of magnitude ($\approx H Ra^{-1/4}$). The duration of the transient, t_b , is obtained by dividing the thermal inertia of the entire enclosure, $(k_f/\alpha)HLW\Delta T$, by the end heat transfer rate, $kHW\Delta T/\delta$. For the experiments studied herein, Table 1 depicts the duration of the transient for three different Rayleigh numbers calculated and it compares the results with those obtained directly from the experiments shown in Fig. 8. The agreement in both trend and magnitude seems good.

The difference in number is quite obvious because the flow in three-dimensional enclosures is essentially different from that in the two-dimensional cavity. The internal wave motion seems to be expected in Fig. 8 at an early phase ($t < 6$ min) for three Rayleigh numbers. According to Patterson and Imberger [8], for $Ra > (Pr/A_H)^4$ one should observe an internal wave motion with the following frequency:

$$\omega = \frac{N}{[1 + (A_H)^2]^{1/2}} \quad (4)$$

where N is known as the Brunt–Vaisala frequency [10] and has the form:

$$N = \frac{(\alpha v Ra)^{1/2}}{H^2} \quad (5)$$

With equations (4) and (5), the internal wave motion gives the corresponding period of the oscillation listed in Table 2 for the present three Rayleigh numbers and compared with those observed from Fig. 8. Again, the trend coincides with those predicted, but the difference in magnitude seems to be due to geometry changes. Based on the above findings, it appears that the period of the internal wave for three-dimensional enclosures is higher than that for two-dimensional cases, and also for the thermal boundary layer development period t_b .

4.4. Heat transfer rate

The Nusselt number was evaluated at the hot wall Nu and it is defined as

$$Nu = \delta \theta_H / \hat{c} x^+ \quad (6)$$

Figure 9 shows the results indicating progression of the flow to steady state for three different Ra values. It can be seen that steady state was finally reached at 36.2, 43.1 and 53.3 for the three corresponding Ra values. For these three Ra values the increased steady-state values indicate the increased importance of convection as Ra increases. Evidence of internal motion is found at $Ra \geq 6.9 \times 10^7$. Generally, the Nusselt numbers at the hot wall monotonically approach a constant value as the thermal boundary layer progresses across the enclosure and the temperature gradients drive an extremely strong circulation, particularly for $Ra = 4.12 \times 10^8$ which results in a high velocity, the presence of a boundary layer and a divergence of the intrusion layer as they enter the core (indicated by the tilt in streak flow patterns). Finally, the streak patterns and isotherms are nearly parallel in the core, showing the dominance of convection. Also shown in Fig. 9 is a comparison of the present results with those of previous investigators for both the transient case [2] and steady-state results [11, 12]. It is found that the agreement for steady-state results is extremely good but the transient results seem much higher than the corresponding numerical prediction, which perhaps indicates that the numerical model for three-dimensional enclosures reported by Fusegi *et al.* [2] is not adequate, although the working fluids used in these two studies are different. They still need improvement and further assessment.

Another important feature of the temporal behavior of the Nusselt number at the hot wall is the pronounced oscillations happening at three different Ra values. The basic mechanism for this oscillating nature was described in detail and discussed in ref. [8]. These oscillations reflect the presence of internal waves. The periods of oscillations are 30, 22 and 14 min for the three corresponding Ra values. The present experimental observations strongly support the existence of such oscillations in three-dimensional situations. However, the periods observed are much higher than that of Fusegi *et al.* [2] (≈ 5.3 min at

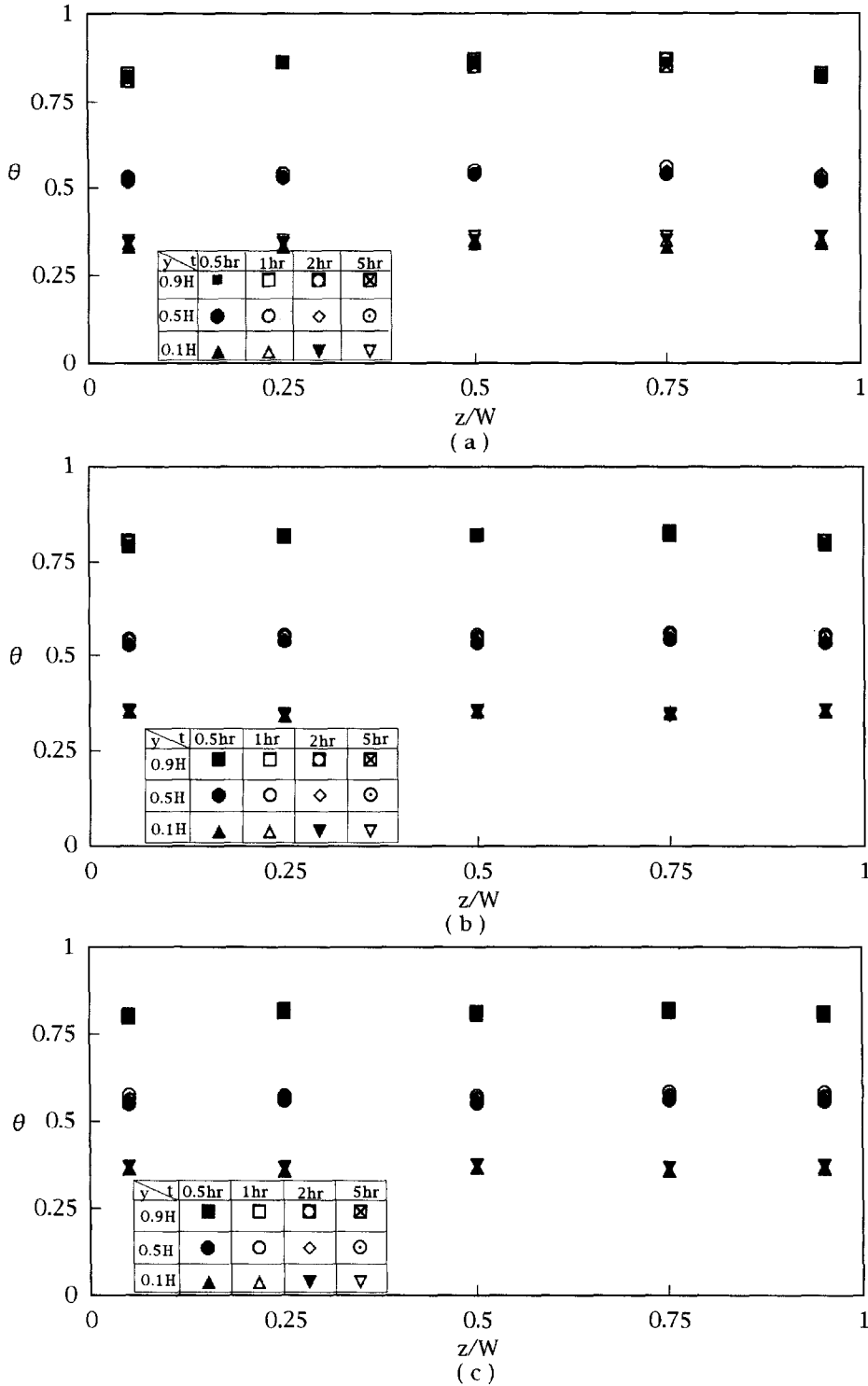


Fig. 7. Centered plane ($x = 0.5L$) time-dependent temperature distribution ($0.5 \leq t \leq 5$ h) for $A_w = 1.2$ and $A_H = 3$ at $y = 0.1H$, $0.5H$ and $y = 0.9H$ for three different Rayleigh numbers: (a) $Ra = 6.9 \times 10^7$; (b) $Ra = 1.38 \times 10^8$; (c) $Ra = 4.12 \times 10^8$.

$Ra = 10^6$) in which numerical results for transient three-dimensional natural convection in a differentially heated cubical enclosure were reported. Such a quantitative comparison can be seen in Fig. 9.

5. CONCLUSION

Transient three-dimensional natural convection in a rectangular enclosure were studied experimentally

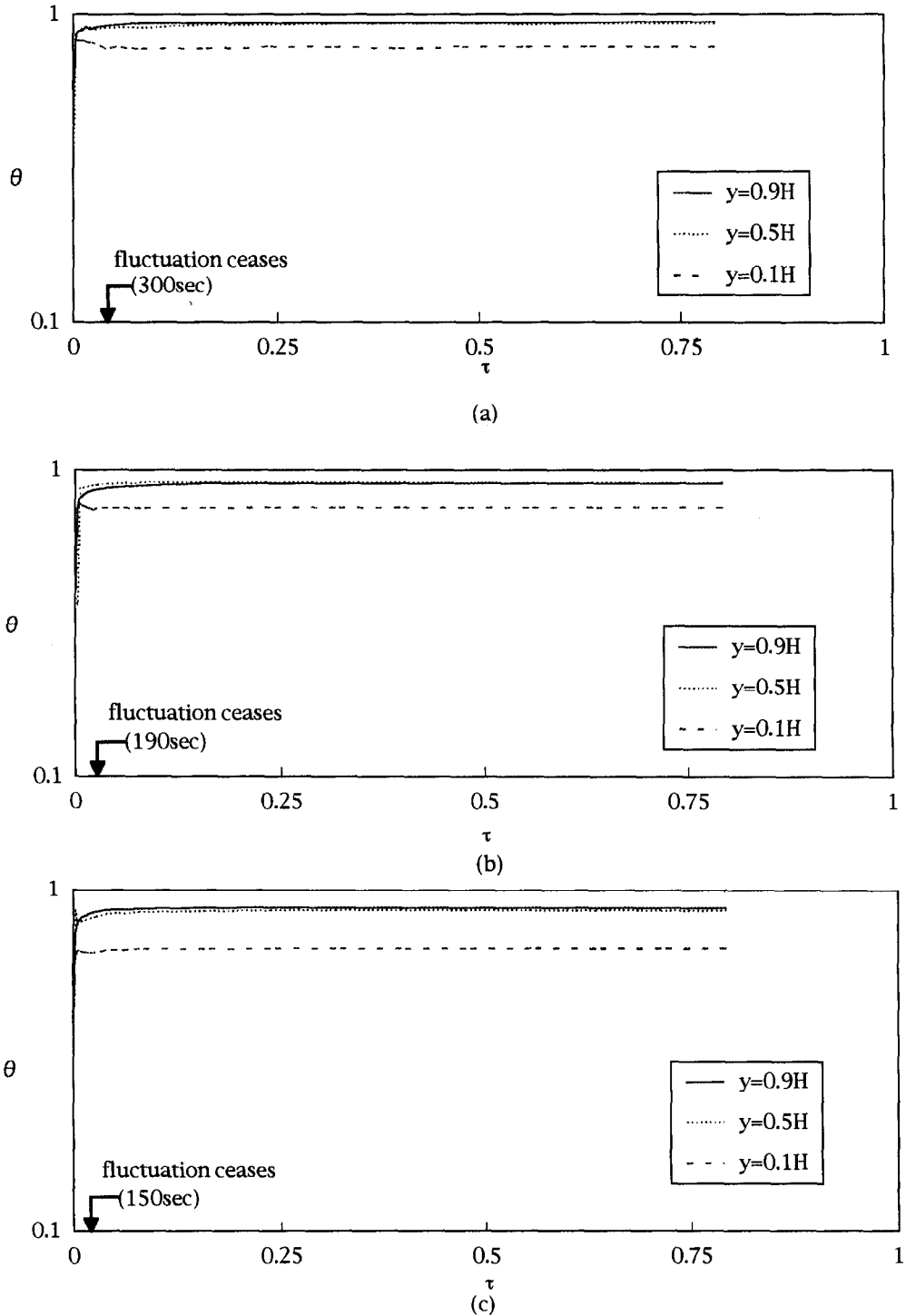


Fig. 8. Midplane ($z = 0.5W$) time-dependent temperature distribution near the hot wall for different elevations: (a) $Ra = 6.9 \times 10^7$; (b) $Ra = 1.38 \times 10^8$; (c) $Ra = 4.12 \times 10^8$.

at Rayleigh numbers of 6.9×10^7 – 4.12×10^8 for aspect ratios of $A_H = 3$ and $A_w = 1.2$ with silicone oil as the working medium. The cell tested had one heated and cooled vertical wall. The four remaining walls were adiabatic. Time evolutions of flow fields through flow visualization and temperature distribution measure-

ments were illustrated by the development of distinct boundary layers along the isothermal walls and the near-stagnant interior core. It was found that the oscillations due to internal waves of the convection flows still exist and the period of the oscillations appears to be about six times higher than those from the ana-

Table 2. Duration of transient and internal wave period for three different Rayleigh numbers and comparisons with previous investigators (two-dimensional enclosures)

	Predicted values $\left(t_b = \frac{H^2}{A_H \alpha Ra^{1.4}}\right)$	Experimental values (t_b)	Equation (5) [s ⁻¹]	Equation (4) [s ⁻¹]	$\Gamma = 2\pi/\omega$ [s]	Fluctuation ceases [s]
$Ra = 6.9 \times 10^7$	13.7 min	50 min	0.826	0.261	24	300
$Ra = 1.38 \times 10^8$	11.5 min	41 min	1.17	0.37	17	190
$Ra = 4.12 \times 10^8$	8.8 min	33 min	2.02	0.639	9.8	150
$Ra = 1.28 \times 10^9$	3.7 h	3.8 h	0.55	0.55	11.5	NA†

Yewell *et al.* [9]

† NA, not available

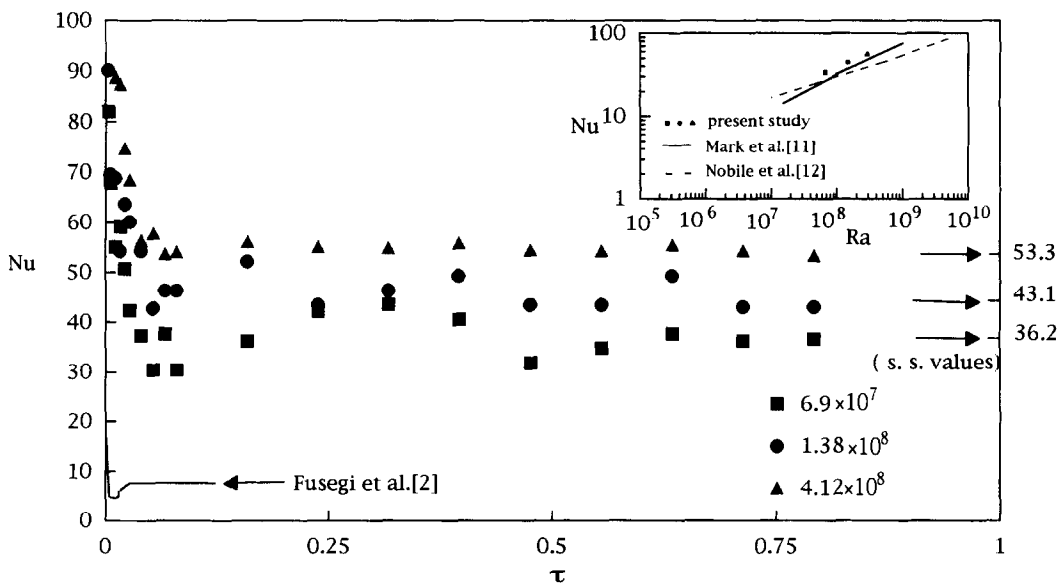


Fig. 9. The dependence of hot wall Nusselt number on τ and comparisons with previous investigations [11, 12].

lytical prediction of two-dimensional flows at $Ra = 10^6$. Three-dimensional steady-state Nusselt number results seem a little higher than those of two-dimensional experiments. Moreover, streak flow patterns strongly suggest that there is a three-dimensional effect in the enclosure at $Ra = 4.12 \times 10^8$ and the working medium such as silicone oil does affect the transient flow behavior, due to its viscosity changes across the enclosure. In spite of the different working fluids used between the previous study and this study, the previous three-dimensional numerical predictions still seem to underestimate the heat transfer rates and extensive experimental data for all kinds (rectangular/cubical) of three-dimensional enclosures are necessarily gathered in a further study.

REFERENCES

1. S. G. Schladow, J. C. Patterson and R. L. Street, Transient flow in a side-heated cavity at high Rayleigh number: a numerical study, *J. Fluid Mech.* **200**, 121–148 (1989).
2. T. Fusegi, J. M. Hyun and K. Kuwahara, Transient three-dimensional natural convection in a differentially heated cubical enclosure, *Int. J. Heat Mass Transfer* **34**, 1559–1564 (1991).
3. S.-S. Hsieh and C.-R. Wang, Experimental study of three-dimensional natural convection in enclosures with different working fluids, *Int. J. Heat Mass Transfer* **37**, 2687–2698 (1994).
4. R. K. Macgregor and A. F. Emery, Free convection through vertical plane layers—moderate and high Prandtl number fluids, *J. Heat Transfer* **91**, 391–404 (1969).
5. Z. Y. Zhong, K. T. Yang and J. R. Lloyd, Variable property effects in laminar natural convection in a square enclosure, *J. Heat Transfer* **107**, 133–138 (1985).
6. J. E. Hart, Stability of the flow in a differentially heated inclined slot, *J. Fluid Mech.* **161**, 161–173 (1985).
7. K. Kublbeck, G. P. Merker and J. Straub, Advanced numerical computation of two-dimensional time-dependent free convection in cavities, *Int. J. Heat Mass Transfer* **23**, 203–217 (1980).

8. J. C. Patterson and J. Imberger, Unsteady natural convection in a rectangular cavity, *J. Fluid Mech.* **100**, 65–86 (1980).
9. R. Yewell, D. Poulidakos and A. Bejan, Transient natural convection experiments in shallow enclosure, *J. Heat Transfer* **104**, 533–538 (1982).
10. J. S. Turner, *Bouyancy Effects in Fluids*, p. 11. Cambridge University Press, Cambridge (1979).
11. N. C. Markatos and K. A. Pericleous, Laminar and turbulent convection in an enclosed cavity, *Int. J. Heat Mass Transfer* **27**, 755–772 (1984).
12. E. Nobile, A. C. M. Sousa and G. S. Barozzi, Turbulent buoyant flows in enclosures, *Proceedings of the Ninth International Heat Transfer Conference*, Vol. 2, pp. 543–548 (1990).